Assessment of different computational models for generation of x-ray spectra in diagnostic radiology and mammography

M. R. Ay[a)]
Department of Physics & Nuclear Sciences, AmirKabir University of Technology, Tehran, Iran, and Division of Nuclear Medicine, Geneva University Hospital, 1211 Geneva, Switzerland

S. Sarkar
Department of Medical Physics, Tehran University of Medical Science & RCSTIM, Tehran, Iran

M. Shahriari
Department of Nuclear Engineering, Shahid Beheshti University, Tehran, Iran

D. Sardari
Department of Physics & Nuclear Sciences, AmirKabir University of Technology, Tehran, Iran

H. Zaidi
Division of Nuclear Medicine, Geneva University Hospital, 1211 Geneva, Switzerland

(Received 12 November 2004; revised 8 February 2005; accepted for publication 19 March 2005; published 24 May 2005)

Different computational methods based on empirical or semi-empirical models and sophisticated Monte Carlo calculations have been proposed for prediction of x-ray spectra both in diagnostic radiology and mammography. In this work, the x-ray spectra predicted by various computational models used in the diagnostic radiology and mammography energy range have been assessed by comparison with measured spectra and their effect on the calculation of absorbed dose and effective dose (ED) imparted to the adult ORNL hermaphroditic phantom quantified. This includes empirical models (TASMIP and MASMIP), semi-empirical models (X-rayb&m, X-raytbc, XCOMP, IPEM, Tucker *et al.*, and Blough *et al.*), and Monte Carlo modeling (EGS4, ITS3.0, and MCNP4C). As part of the comparative assessment, the K x-ray yield, transmission curves, and half value layers (HVLs) have been calculated for the spectra generated with all computational models at different tube voltages. The measured x-ray spectra agreed well with the generated spectra when using X-raytbc and IPEM in diagnostic radiology and mammography energy ranges, respectively. Despite the systematic differences between the simulated and reference spectra for some models, the student's *t*-test statistical analysis showed there is no statistically significant difference between measured and generated spectra for all computational models investigated in this study. The MCNP4C-based Monte Carlo calculations showed there is no discernable discrepancy in the calculation of absorbed dose and ED in the adult ORNL hermaphroditic phantom when using different computational models for generating the x-ray spectra. Nevertheless, given the limited flexibility of the empirical and semi-empirical models, the spectra obtained through Monte Carlo modeling offer several advantages by providing detailed information about the interactions in the target and filters, which is relevant for the design of new target and filter combinations and optimization of radiological imaging protocols.
[DOI: 10.1118/1.1906126]

I. INTRODUCTION

A detailed knowledge of x-ray spectra is required for the mathematical modeling and optimization of imaging systems in diagnostic radiology. The direct measurement of spectra, however, requires expensive equipment and careful attention and planning during the experimental measurement setup,[1–6] which is generally not practical in a clinical diagnostic radiology department with limited physics support. Since direct measurement of x-ray spectra is time consuming and remains a difficult task, attempts for prediction of x-ray spectra in different energy ranges and various target/filter combinations have begun several decades ago and still represent an active research area. Generally the x-ray prediction models can be divided into three categories: empirical,[7–11] semi-empirical,[12–17] and Monte Carlo calculations.[4,18–21]

Empirical models are based on the use of measured data for prediction of x-ray spectra. Early attempts by Silberstein[22] relied on the determination of x-ray spectra from measurement of x-ray attenuation curve. Several groups made every effort to analyze the attenuation data as accurately as possible by different mathematical methods such as analytical modeling,[23] Laplace transform,[24] iterative methods,[11,25] matrix manipulation,[26] and neural networks.[27] Nevertheless, the calculation of x-ray spectra from attenuation curves is subject to errors in two respects. First, attenuation measurement with various detectors will yield different values for the same spectrum due to different response of detectors.[28] Second, it would be possible to calculate different spectra from identical attenuation curves. An alternative

method proposed by Boone *et al.*[9,10] fits the highest order polynomial to the measured spectra without any assumption concerning the physics of x-ray production.

Semi-empirical models are based on a theoretical formulation to calculate the x-ray spectra by mathematical derivation followed by some tuning in the equations' parameters using measured spectra. The earliest theoretical model of differential intensity of the bremsstrahlung was introduced by Kramers.[29] This model was modified later on to include the target attenuation.[23] Birch and Marshal[12] adjusted some parameters in the latter model to give good agreement with experimental data. They used Green's formulation[30] for estimating the characteristic radiation with some modifications using experimental measurements. Iles[14] included a term for electron backscatter from the target to this model whereas Tucker *et al.*[15] modified this model by incorporating appropriate modeling for the fact that the bremsstrahlung and characteristic x rays are produced in different depths in the target. They used the Vignes and Dez[31] approach with some modifications to estimate the characteristic radiations and proposed another model for generating molybdenum target x-ray spectra by extending the tungsten target model.[16] Blough *et al.*[17] proposed a model based on Tucker *et al.*'s work using mathematical formulation instead of semi-empirical functions for production of mammography spectra.

On the other hand, Monte Carlo calculations use direct transport of electrons and generated photons in the target and filter for calculation of x-ray spectra. Monte Carlo simulation has proven to be the most suitable theoretical tool for the computation of x-ray spectra in complex geometries. For this purpose, some groups used self-written or in house developed computer codes,[18] while others used public domain general-purpose Monte Carlo codes such as EGS4,[4] MCNP,[19,21,32] and ITS.[20]

The spectra predicted with the aforementioned models do not have the same bremsstrahlung x-ray energy distribution and characteristic x-ray intensity, even for the same tube voltage and target angle. Thus, the accuracy of predicted spectra with these methods should be investigated considering the impact they might have on performance parameters of diagnostic radiological imaging systems and radiation dosimetry calculations. A few publications addressed the issue of comparing various methods proposed for calculating x-ray spectra; however, none of them covered all existing computational models using different target/filter combinations for various tube voltages in diagnostic radiology and mammography energy range.[33] Bissonnette and Schreiner[34] compared Birch and Marshal[12] with the Tucker *et al.*[15] model while Bhat *et al.*[3] compared the same models with spectra measured with a high-purity germanium detector. Caon *et al.*[35] compared four x-ray prediction methods by calculating the resulting absorbed dose to x-ray computed tomography (CT) body and head phantoms. Ng *et al.*[20] compared Boone *et al.*[9] and IPEM spectra with ITS Monte Carlo simulations in mammography energy range whereas Wilkinson *et al.*[6] compared four methods with measured spectra for molybdenum target.

In this study, the accuracy of spectra generated by empirical models (TASMIP and MASMIP), semi-empirical models (IPEM, X-raytbc, X-rayb&m, XCOMP, Tucker *et al.*, and Blough *et al.*), and Monte Carlo calculations (MCNP4C, EGS4, and ITS3.0) in both the diagnostic radiology and mammography energy ranges are assessed through comparison with measured spectra published by Fewell *et al.*[1,2] for different target/filter combinations and tube voltage parameters. The comparative assessment encompassed many figures of merit including qualitative and quantitative assessment of spectra shape, the difference in K x-ray yield, transmission curves, half value layer (HVL) as well as absorbed dose and effective dose imparted to the adult ORNL hermaphroditic phantom.

II. MATERIALS AND METHODS

A. Experimental measurement of x-ray spectra

The measured spectra published by Fewell *et al.*[1,2] have been used as the gold standard in this study because of their reliability, availability, and popularity among the diagnostic imaging community. Despite the significant advances made in experimental x-ray spectroscopy, the above referenced reports are still the most complete and exhaustive experimental measurements available today. Moreover, the spectra were measured without added filtration, thus giving the opportunity to the user to modify the spectrum using known attenuation properties of any particular material as additional filter.

Measurement of x-ray spectra in diagnostic radiology. The measured spectra used in this study were taken from the Handbook of Computed Tomography X-ray Spectra.[2] The high voltage generator employed in the experiments is the L90-10C Delta ray constant potential with maximum output rating of 180 kV and 10 mA. Published data for the Eimac (B-160-H, A-465) x-ray tube (Ohio Nuclear Inc., Solon, OH) with 12.5° tungsten target angle and nominal inherent filtration of 1.2 mm Al were used. The x-ray spectra were measured with a high-purity germanium detector. The spectrometer was calibrated to give an energy conversion of 0.15 keV per channel. After correction of detector response, the x-ray spectra were tabulated in 2 keV energy bins.

Measurement of x-ray spectra in mammography. The measured spectra used in this study were taken from the Handbook of Mammographic X-ray Spectra.[1] The General Electric MSI-1250II high voltage generator was used, which can operate as a three-phase, 12-pulse system in the radiologic mode and as a single phase full rectified system in the fluoroscopy mode. The ripple in high voltage waveform varied from approximately 4% to 6%. The tabulated spectra in the 1 keV energy bin for Dynamax M64 molybdenum and Dynamax 69M tungsten target x-ray tube (Machlett Laboratories, Stamford, CT) with inherent filtration of 0.6 mm A1 and 12° target angle were used as reference spectra in this study. Similar to the diagnostic energy range, the x-ray spectra were measured with high-purity germanium detector.

B. Empirical models

TASMIP. This model uses interpolating polynomials to compute the x-ray spectra at 1 keV energy bin for tube voltages between 30 and 140 kV for a tungsten target from a modified version of Fewell's measured spectra as a data source.[7] The highest order polynomial that is practical (depending on the number of data points available in the fit) has been used for fitting the data. The various tube voltage ripples and aluminum filters have been considered in this model.[10]

MASMIP and TASMIP. These computer models were developed for generating x-ray spectra in the mammographic energy range from 18 to 40 kV through an interpolating polynomial method in 0.5 keV energy bins. The tungsten and molybdenum anode spectral models are named TASMIP and MASMIP, respectively.[9] Different sets of polynomials have been used for each anode material (Mo and W). It is worth emphasizing that these models are not able to predict the x-ray spectra for various combinations of targets/filters (and their thicknesses) and anode angles.

TABLE I. Summary of computational models used for generation of x-ray spectra in diagnostic radiology and mammography energy range assessed in this study.

Computational model	Category	Target material	Reference
Measurement[a]	Experimental	W	2
Measurement[b]	Experimental	W, Mo, W/Mo	1
TASMIP[a,b]	Empirical	W	10
MASMIP[b]	Empirical	Mo	9
X-rayb&m[a,b]	Semi-empirical	W	12
IPEM[a,b]	Semi-empirical	W, Mo, Rh	38
XCOMP[a,b]	Semi-empirical	W	13
X-raytbc[a,b]	Semi-empirical	W	15
Tuckeret *et al.*[b]	Semi-empirical	Mo	16
Bloughet *et al.*[b]	Semi-empirical	W, Mo, Rh	17
MCNP4C[a,b]	Monte Carlo	All materials	39
EGS4[a,b]	Monte Carlo	All materials	40
ITS3.0[a,b]	Monte Carlo	All materials	41

[a]Radiology energy range.
[b]Mammography energy range.

C. Semi-empirical models

XCOMP. This computer program can be used for calculation of x-ray spectra, kerma, and HVL for various tube settings (kV, anode angle, distance) and eight absorbing materials (Be, Al, Cu, Sn, Pb, PMMA, water, and oil) with different thicknesses according to Birch and Marshal model.[13] The tube voltage can be selected between 20 and 150 kV in 0.1 kV steps. The energy bin is set to 0.5 keV for voltages less than 50 kV and 1 keV for tube voltages between 50 and 150 kV.

IPEM Report No. 78. The original version of the catalog was published in 1979 and provided essential data useful for applications in diagnostic radiology and mammography.[36] The current version uses XCOM program[37] to calculate linear attenuation coefficients for various materials and contains sets of radiology and mammography x-ray spectra with much wider ranges than the previous version. The spectra are presented for tungsten targets at tube voltages from 30 to 150 kV and target angles from 6° to 22° at 1° intervals. Constant potential mammographic spectra are provided from 25 to 32 kV for molybdenum and rhodium targets for target angles ranging between 9° and 23°. Different materials can be used as additional filters. All spectra are provided at an energy interval of 0.5 keV.[38]

X-raytbc and X-rayb&m. These models (computer program supplied by Dr. G. Stirling NRL, Christchurch, New Zealand) predict the x-ray spectra, kerma, and HVL for various tube voltages, anode angles, distances, and absorbing materials (Be, Al, Cu, Pb, water, oil, pyrex glass, lexan, concrete, cortical Bone, soft tissue, and acrylic) in the range 10 to 150 kV for constant and two pulse tube voltages. The energy bin is set to 1 keV for both models. Attenuation coefficients are taken from five sources depending on material composition. X-raytbc is based on the Tucker *et al.*[15] model for tungsten-rhenium alloy target (90/10 atomic percent W/Re alloy) while X-rayb&m is based on the Birch and Marshall[12] model for tungsten target.

Tucker et al. model. This semi-empirical model generates x-ray spectra in a molybdenum target and takes into account the depth of production for both bremsstrahlung and characteristic x rays.[16] The computer program written by Wilkinson *et al.*[6] was used in this work.

Blough et al. model. This analytical model was developed to allow calculation of mammographic spectra in various target and filter combinations.[17] It uses the same formulation of Tucker *et al.*[16] except that a semi-empirical mathematical polynomial derivation was used instead of fitting measured data.[15,16] The spectra published by Wilkinson *et al.*[6] for a molybdenum target were used in this study.

D. Monte Carlo modeling

MCNP4C. The Monte Carlo N-Particle version 4C (MCNP4C) is a general-purpose Monte Carlo code that can be used for neutron, photon, and electron or coupled neutron/photon/electron transport. For simulation of x-ray spectra, MCNP4C was run in photon and electron mode (mode: P,E). A continuous slowing down model is used for electron transport. Photon transport in diagnostic radiology energy range includes photoelectric absorption with creation of K- and L-shell x-ray photons or Auger electrons and coherent and incoherent scattering.[39] An in-depth description of the use of this code for x-ray spectra simulation is given elsewhere.[19]

EGS4. The Electron-Gamma Shower version 4 (EGS4) is a general purpose Monte Carlo code for transport of electrons and photons in arbitrary geometry and media for particles with energies from a few keV up to several TeV.[40] The general particle transport physics in this code is the same as MCNP4C except that the latter includes the production of characteristic photons by electron impact ionization.[21] The data simulated by Bhat *et al.*[4] were used in this work.

ITS3.0. The Integrated TIGER Series version 3 (ITS3.0)

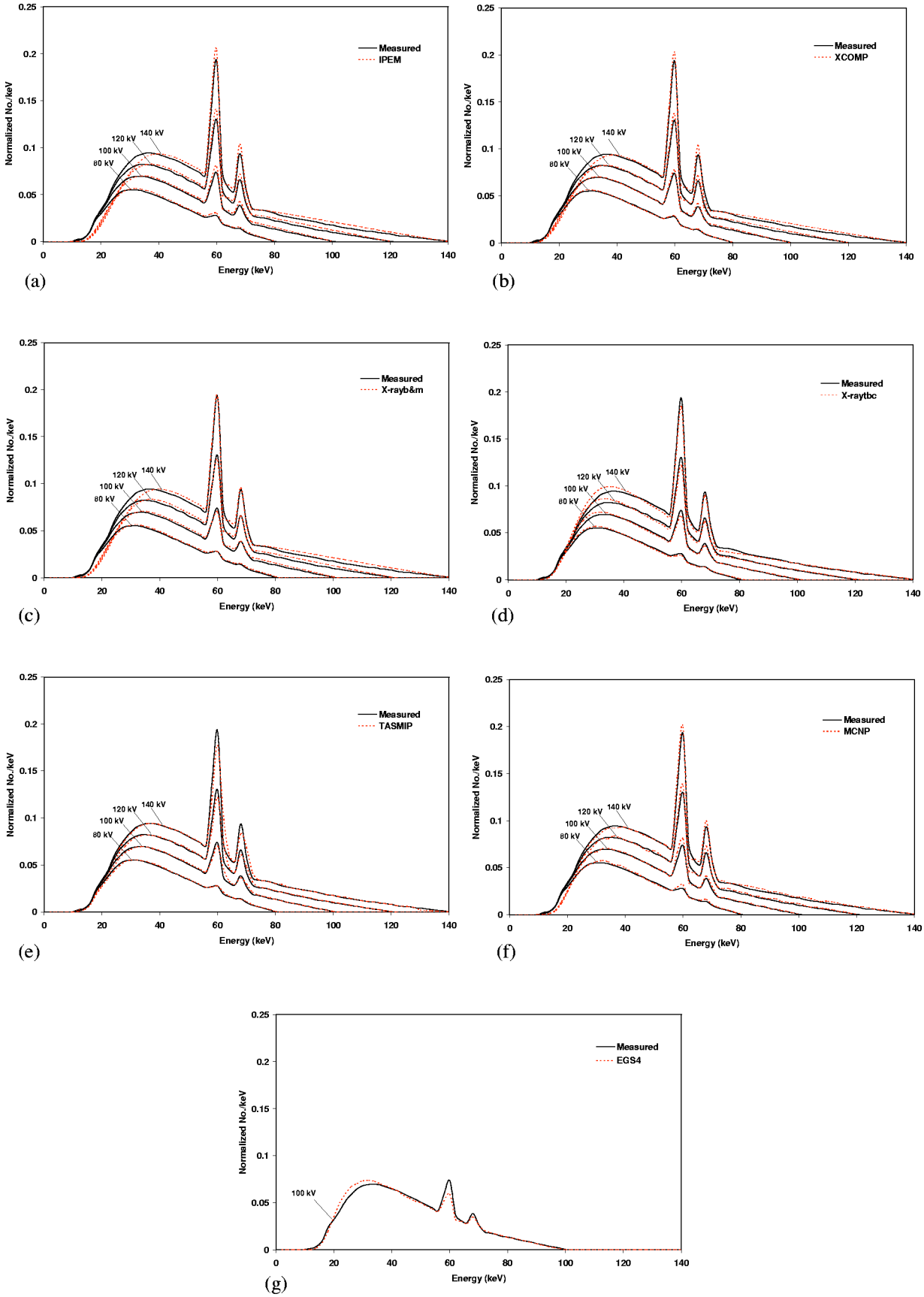

FIG. 1. Comparison of x-ray spectra calculated using the different computational models with measured spectra at tube voltages between 80 and 140 kV for 12.5° tungsten target, 1.2 mm Al_{eq} inherent filter, and FSD 127 cm.

TABLE II. Ratios of total tungsten K x rays to sum of bremsstrahlung and K x rays using various computational models for different tube voltages.

Computational model	80 kV		100 kV		120 kV		140 kV	
	Total	Difference[a] (%)	Total	Difference (%)	Total	Difference (%)	Total	Difference (%)
Measured	0.012 50	na[b]	0.046 28	na	0.071 96	na	0.091 13	na
IPEM	0.015 72	−25.7	0.053 96	−16.6	0.081 81	−13.7	0.101 07	−10.9
XCOMP	0.015 01	−20.1	0.051 97	−12.3	0.079 91	−11.0	0.099 69	−9.4
X-rayb&m	0.010 90	12.8	0.040 90	11.6	0.068 35	5.0	0.090 13	1.1
X-raytbc	0.010 67	14.6	0.039 95	13.7	0.064 72	10.1	0.084 62	7.1
TASMIP	0.012 32	1.4	0.043 58	5.8	0.068 69	4.5	0.085 60	6.0
MCNP4C	0.020 97	−67.8	0.055 67	−20.3	0.080 02	−11.5	0.098 50	−8.1
EGS4	⋯	⋯	0.033 46	27.7	⋯	⋯	⋯	⋯

[a]Relative difference with measured spectra.
[b]Not applicable.

of coupled electron/photon Monte Carlo code is a powerful tool for determining state-of-the-art descriptions of the production and transport of the electron/photon cascade in a time-independent, multi-material, and multi-dimensional environment.[41] The ITS-simulated spectra in this study were taken from Ng *et al.*[20]

E. Comparative assessment strategy

The x-ray spectra calculated by the different computational models summarized in Table I were assessed through comparison with measurement spectra. The criteria and figures of merit used include spectrum shape, attenuation curves, HVLs, K x-ray yield, absorbed dose, and effective dose in the adult ORNL hermaphroditic phantom.[42] Note that the spectrum shape is the best parameter for qualitative visual assessment of potential differences between two spectra owing to the fact that it includes the bremsstrahlung and characteristic x rays. On the other hand, attenuation curves and HVLs are standard indices of beam quality while the K x-ray yield indicates the contribution of characteristic x rays to the total spectrum. Finally, the calculation of the absorbed dose gives an indication of the impact of x-ray spectra on energy imparted to the irradiated phantoms, which is useful for clinical and research applications.

Since the spectra shape and beam quality are a function of tube voltage, filtration, and anode angle, the different computational models were used to simulate spectra with the same parameters used in experimental measurements. The energy bin of the spectra produced by the computational models was changed to 2 keV in radiology and 1 keV in mammography for comparison with measured spectra.[1,2] The calculation of HVLs and transmission curves was performed using the original energy bin. During the rebinning process, the resulting spectra for some computational models do not fall to zero at maximum tube voltage. Quantitative evaluation of the differences between measured spectra and the spectra generated by different models was performed using the root mean square difference (RMSD) metric and statistical student's *t*-test analysis. The transmission curves were calculated by dividing the transmitted air kerma through the filter by the air kerma without the filter being present. The HVLs and transmission curves calculated for some models in this study have small differences in some cases with the values reported by the original codes. This can be attributed to differences in attenuation coefficients for aluminium, which are derived from XCOM program[37] in our work. The K x-ray contribution is determined by subtracting the bremsstrahlung part of the spectra form total counts in the desired region and normalizing to the total number of photons in the spectra. The bremsstrahlung spectra can be obtained by subtracting the K x-ray yields from the appropriate intervals in the spectra.[2]

The MCNP4C Monte Carlo code was used for calculation of absorbed dose in ORNL hermaphroditic phantom. The predicted spectra using the different computational models at 100 kV were used as input. The x-ray source was set at a distance of 100 cm from the chest of the ORNL hermaphroditic phantom. A field of view (FOV) of 40×40 cm^2 was considered and 1.5×10^7 photons were employed in the simulation to get an uncertainty less than 1% in the calculation of absorbed dose using *F6 tally, which calculates the energy deposit averaged over a cell. No variance reduction technique was used and all photon interactions were simulated until they are absorbed in the phantom or escape from it. The ED was calculated using appropriate tissue weighting factors.[43] The same simulations were performed for molybdenum and tungsten target mammographic spectra at 30 kV to calculate the mean absorbed dose to the breasts ($\overline{D_b}$) and ED using typical mammography setup (FSD 50 cm, FOV 10×10 cm^2). The values calculated by Monte Carlo simulation were scaled to mimic typical values encountered in chest and mammography x-ray imaging for measured spectra that is an ED of 40 μSv for x-ray chest imaging and a mean absorbed dose to breasts of 2 mGy in mammography.[44]

III. RESULTS

A. Diagnostic radiology

Figure 1 shows the comparison of tungsten x-ray spectra calculated using different computational models with measured spectra for an Eimac x-ray tube at tube voltages between 80 and 140 kV, except the spectra calculated using

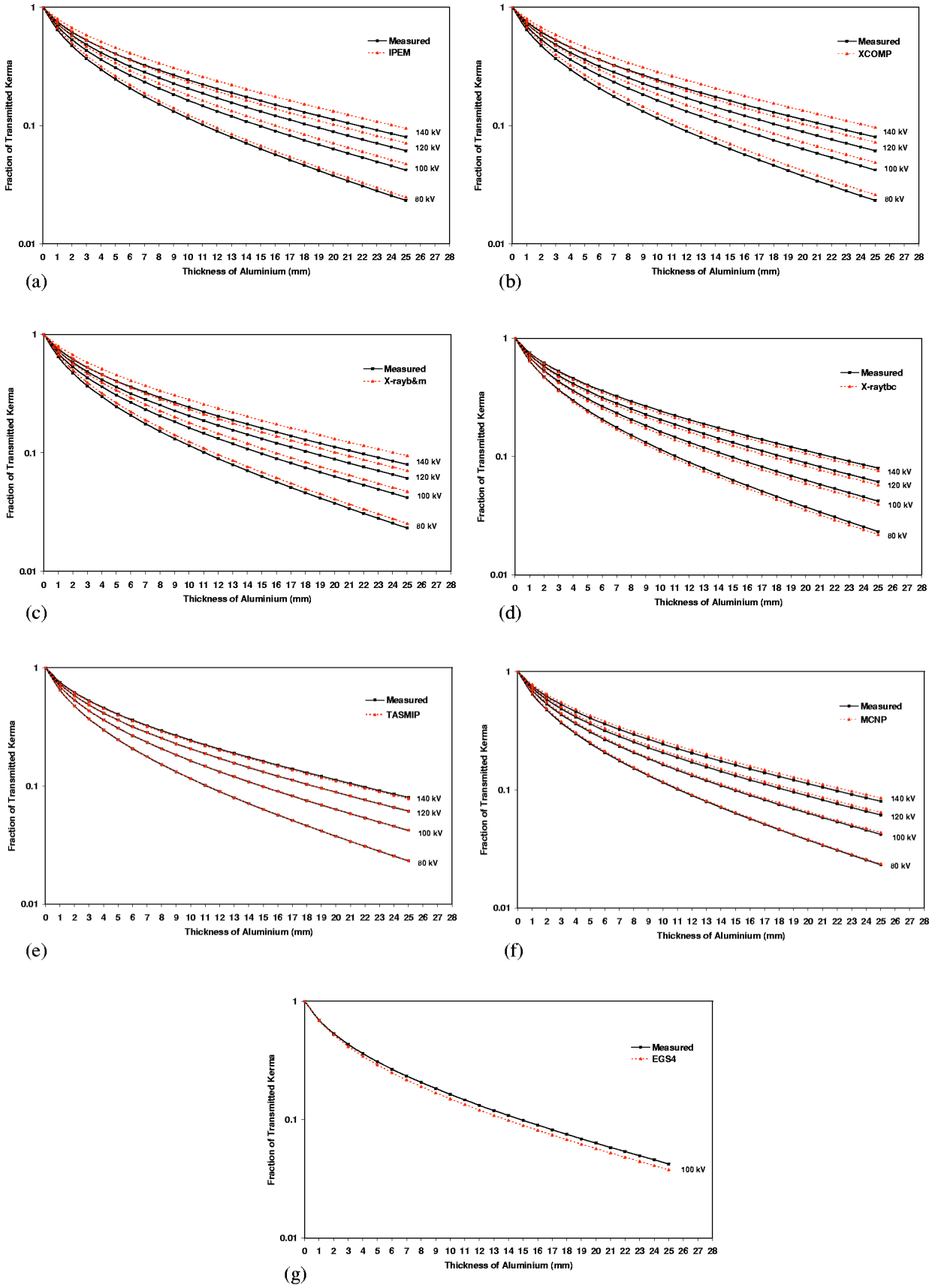

FIG. 2. Comparison of transmission curves produced by different computational models with those calculated from measured spectra at tube voltages between 80 and 140 kV for 12.5° tungsten target, 1.2 mm Al_{eq} inherent filter, and FSD 127 cm.

TABLE III. Comparison of maximum and mean absolute relative difference between transmission curves calculated using the different computational models and curves calculated from measured spectra (12.5° tungsten target, 1.2 mm Al_{eq} inherent filtration).

Computational model	80 kV		100 kV		120 kV		140 kV	
	Mean (%)	Max (%)	Mean (%)	Max (%)	Mean (%)	Max (%)	Mean (%)	Max (%)
IPEM	7.6	9.2	10.4	12.7	13.1	16.3	14.9	18.6
XCOMP	9.5	11.9	12.3	15.8	14.4	18.1	16.1	20.6
X-rayb&m	6.2	6.9	9.9	12.4	12.2	15.8	14.6	18.6
X-raytbe	4.1	5.6	4.5	6.1	4.7	6.1	3.7	5.2
TASMIP	0.5	0.8	0.6	1.2	0.5	1.3	1.7	2.4
MCNP	2.0	2.7	3.0	3.5	4.4	5.6	5.5	6.8
EGS4	⋯	⋯	7.7	10.3	⋯	⋯	⋯	⋯

EGS4 which are available only at 100 kV. All spectra were normalized to the total number of photons in each spectrum. The relative difference between measured and calculated total K x rays is summarized in Table II. Good agreement between the bremsstrahlung x rays produced by the TASMIP model with measured spectra can be observed while the characteristic x rays have lower intensity. The relative difference of total K x-ray yields with measured data increase with increasing tube voltage. In comparison with measured spectra, all semi-empirical models based on Birch and Marshal theory[12] have lower intensity at low energies while they have higher intensity in high energies ($E>68$ keV) for all tube voltages. Our calculations showed that the K x-ray yield in all peaks ($K_{\alpha 1}, K_{\alpha 2}, K_{\beta 1}, K_{\beta 2}$) in both IPEM and XCOMP is higher than measured spectra while these values are lower in X-rayb&m model. The total K x-ray yield values shown in Table II indicate that these differences decrease with increasing tube voltage. The X-raytbc model based on Tucker *et al.*[15] theory produces more low energy x rays ($E<42$ keV) and the intensity of characteristic x rays predicted by this model is lower than measured spectra in all peaks. The calculated spectra by MCNP have higher intensity in low energy photons while this behavior is reversed for energies >68 keV in comparison with measured spectra. The K x-ray yields have higher intensity in all energies. The relative difference of total K x-ray yields decreases by increasing tube voltage. The low energy bremsstrahlung photons have higher intensity in the spectra simulated by EGS4 at 100 kV in comparison with measured spectra, while this behavior is reversed for the intensity of characteristic x rays.

The quality of x-ray spectra calculated with different computational models as compared to measured spectra was assessed in Fig. 2, which shows the transmission curves through aluminum filter for different tube voltages. All models based on Birch and Marshal theory (IPEM, XCOMP, and X-ray&m) result in higher transmission curves in comparison with measured spectra for all tube voltages and the difference increases with increasing the tube voltage. This behavior is reversed for transmission curves calculated using X-raytbc, while the transmission curves calculated using TASMIP spectra have good agreement with the curves calculated from measured spectra. The transmission curves calculated using MCNP spectra have higher values and this difference increases with increasing tube voltage, whereas the EGS4 transmission curve has lower values in comparison with measured spectra. Table III shows the maximum and

TABLE IV. Comparison of root mean square difference (RMSD) between measured and calculated spectra using the different computational models (the original data values have been multiplied by 10^3).

Computational model	Figure 1				Figure 3		Figure 5		
	80 kV	100 kV	120 kV	140 kV	25 kV	30 kV	30 kV	35 kV	40 kV
IPEM	2.66	3.84	5.17	6.34	5.69	14.87	7.53	8.04	8.10
XCOMP	1.01	1.89	3.18	4.56	⋯	⋯	10.09	8.06	9.67
X-rayb&m	2.37	3.31	4.45	5.53	⋯	⋯	9.06	14.87	14.24
X-raytbe	0.98	1.83	2.67	3.03	⋯	⋯	10.20	16.88	17.44
TASMIP	1.24	2.04	3.40	5.06	⋯	⋯	8.64	7.39	9.94
MCNP4C	2.18	2.70	3.20	3.62	27.89	30.47	11.68	8.84	11.64
EGS4	⋯	3.66	⋯	⋯	⋯	⋯	⋯	⋯	⋯
Blough *et al.*	⋯	⋯	⋯	⋯	20.55	20.61	⋯	⋯	⋯
Tucker *et al.*	⋯	⋯	⋯	⋯	11.90	16.50	⋯	⋯	⋯
MASMIP	⋯	⋯	⋯	⋯	4.29	10.67	⋯	⋯	⋯
ITS3.0	⋯	⋯	⋯	⋯	⋯	14.18	9.90	⋯	⋯

TABLE V. Comparison between measured and computed HVL estimates (in mm Al) using the different computational models for tube voltages in the diagnostic radiology energy range (12.5° tungsten target, 1.2 mm Al_{eq} inherent filtration).

Computational model	80 kV		100 kV		120 kV		140 kV	
	HVL	Difference (%)	HVL	Difference (%)	HVL	Difference (%)	HVL	Difference (%)
Measured	1.81	na	2.29	na	2.81	na	3.36	na
IPEM	2.02	−11.6	2.67	−16.5	3.41	−21.3	4.22	−25.5
SCOMP	2.03	−12.1	2.68	−17.0	3.44	−22.4	4.27	−27.1
X-rayb&m	2.01	−11.0	2.65	−15.7	3.39	−20.6	4.20	−25.0
X-raytbe	1.78	1.6	2.22	3.0	2.73	2.8	3.29	2.1
TASMIP	1.81	0	2.29	0	2.81	0	3.30	1.8
MCNP4C	1.86	−2.8	2.40	−4.8	2.95	−5.0	3.62	−7.7
EGS4	⋯	⋯	2.15	6.1	⋯	⋯	⋯	⋯

mean differences between measured and calculated transmission curves. It can be seen that the percentage absolute value of maximum and mean relative errors in transmission curves calculated from XCOMP spectra are higher than the other models for energies between 80 and 140 kV. Table IV summarizes the root mean square difference between measured and calculated spectra for the different computational models in different energies. It can be seen that the RMSD is minimum for the spectra calculated using the X-raytbc model in the diagnostic radiology energy range.

Further comparative assessment of the quality of x-ray spectra calculated by different models is illustrated in Table V, which shows the calculated HVLs and their relative difference with respect to measured data for tube voltages between 80 and 140 kV. Once again, the difference increases with increasing tube voltage and the XCOMP model has the maximum difference with measured spectra. Note that IPEM and X-rayb&m models produce very close estimates to this latter model. Table VI summarizes the impact of the x-ray spectra on the ED imparted to the ORNL hermaphroditic phantom in typical chest x-ray imaging setup, with 1.2 and 3.2 mm aluminum filters at 100 kV. The maximum differences in calculation of ED in comparison with measured spectra with 1.2 and 3.2 mm Al filters are −3.2% and −5% for IPEM, while the minimum differences are 0% and 0.6% for x-raytbc, respectively.

B. Mammography

Figure 3 shows the comparison of spectra predicted by different computational models with measured spectra published by Fewell *et al.*[1] for a Dynamax M64 x-ray tube at voltages of 25 and 30 kV. All spectra predicted by computational models have higher intensity in the low energy range ($E<15$ keV), although it appears that IPEM and MASMIP produce the same amplitude at low energies compared with measured spectra for 30 kV. The difference in K x-ray characteristic yield was calculated for all peaks; however, only the total value and its relative difference with measured spectra are reported in Table VII. According to these data, MASMIP underestimates the production of characteristic x rays in both tube voltages, while MCNP4C overestimates these values. The maximum difference in production of K x-ray yield with measured spectra are −71.8% and −73.5% at 25 kV and −31.3% and −42.3% at 30 kV for MCNP4C spectra with

TABLE VI. Comparison between MCNP4C-based Monte Carlo calculations of effective dose (ED) in adult ORNL hermaphroditic phantom in typical chest x-ray imaging setup (100 kV, FSD 100 cm, 12.5° target angle) with 1.2 and 3.2 mm Al filter.

Computational model	1.2 mm Al filter		3.2 mm Al filter	
	ED (μSv)	Difference[a] (%)	ED (μSv)	Difference (%)
Measured	40.00±1.4	na	29.81±0.3	na
IPEM	41.30±1.4	−3.2	31.29±0.3	−5.0
XCOMP	40.55±1.4	−1.4	30.55±0.3	−2.5
X-rayb&m	41.11±1.5	−2.8	31.11±0.3	−4.3
X-raytbc	40.00±1.6	0	29.63±0.3	0.6
TASMIP	40.37±1.5	−0.9	30.37±0.3	−1.7
MCNP4C	40.74±1.4	−1.8	30.55±0.3	−2.5
EGS4	39.63±1.4	0.9	29.26±0.3	1.9

[a]Relative difference with calculated effective dose from measured spectrum.

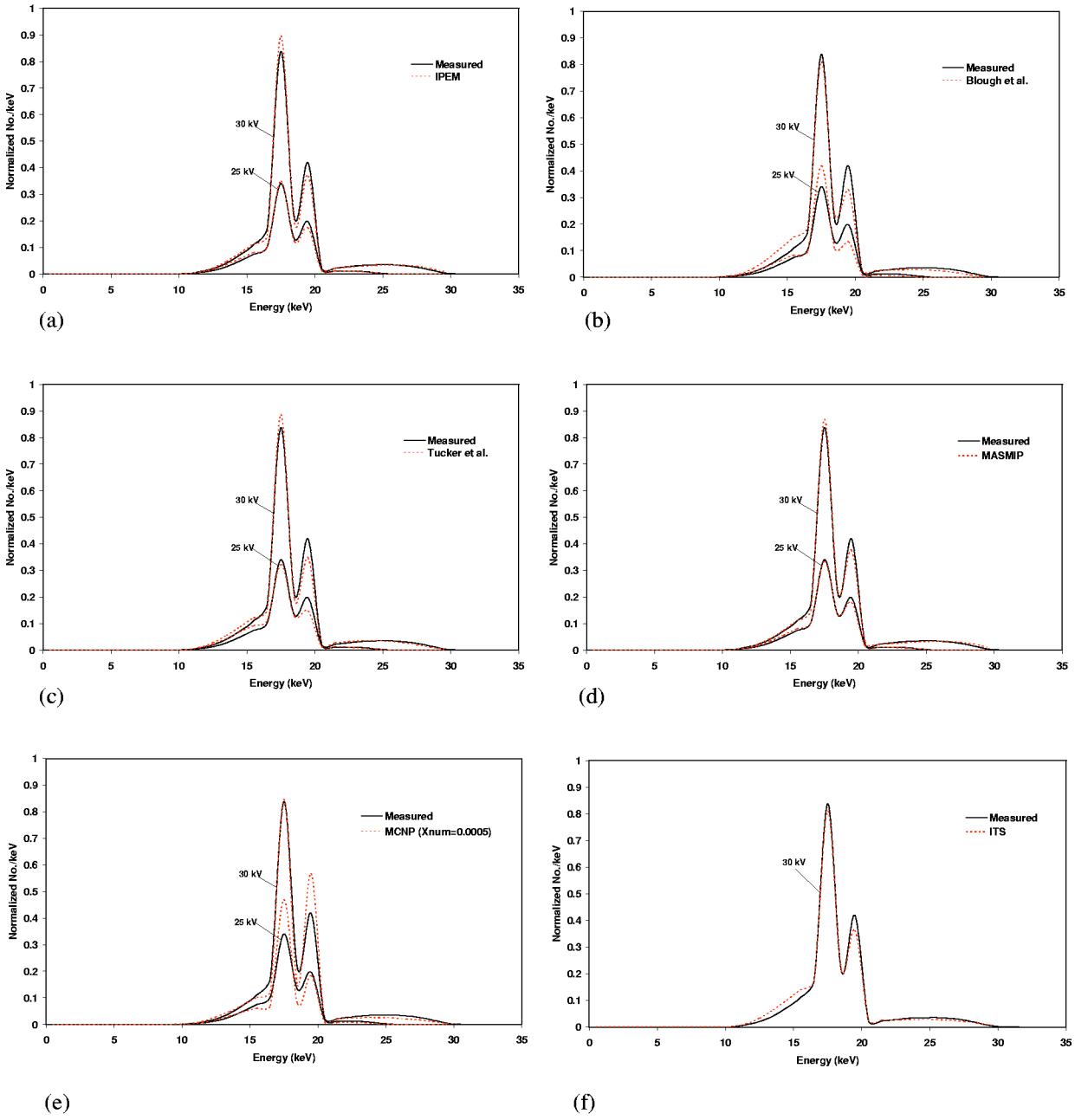

FIG. 3. Comparison of x-ray spectra calculated using different computational models with measured spectra at tube voltages 25 and 30 kV for 12° molybdenum target, 0.6 mm Al_{eq} inherent filter, 0.03 mm Mo additional filter, and FSD 100 cm.

XNUM values of 0.0005 and 1, respectively, whereas the minimum difference is 1.1% (at 25 kV) for IPEM and −0.4% (at 30 kV) for the Tucker *et al.* model.

The quality of produced spectra with different models with respect to transmission curves is assessed in Fig. 4. It can be seen that all models underestimate the measured transmission curves in each filter thickness. Figure 5 shows the comparison between the spectra predicted by different computational models and measured spectra for a Dynamax 69M tungsten target x-ray tube at tube voltages of 30, 35, and 40 kV. The peak of calculated spectra for all models occurs at lower energy in comparison with measured spectra and has lower intensity in all tube voltages, whereas the measured spectra has higher intensity in low and high energies. All transmission curves calculated using different computational models have lower amplitude in comparison with measured spectra at tube voltages 35 and 40 kV while this behavior is reversed at 30 kV, except the curve calculated from ITS (Fig. 6).

The maximum and mean absolute relative differences between measured and calculated transmission curves for molybdenum and tungsten targets are reported in Table VIII. Table IX compares calculated HVLs obtained using the different models with measured spectra at tube voltages 25 and 30 kV for a molybdenum target and 30, 35, and 40 kV for a tungsten target. A maximum difference of 8.6% at 30 kV for

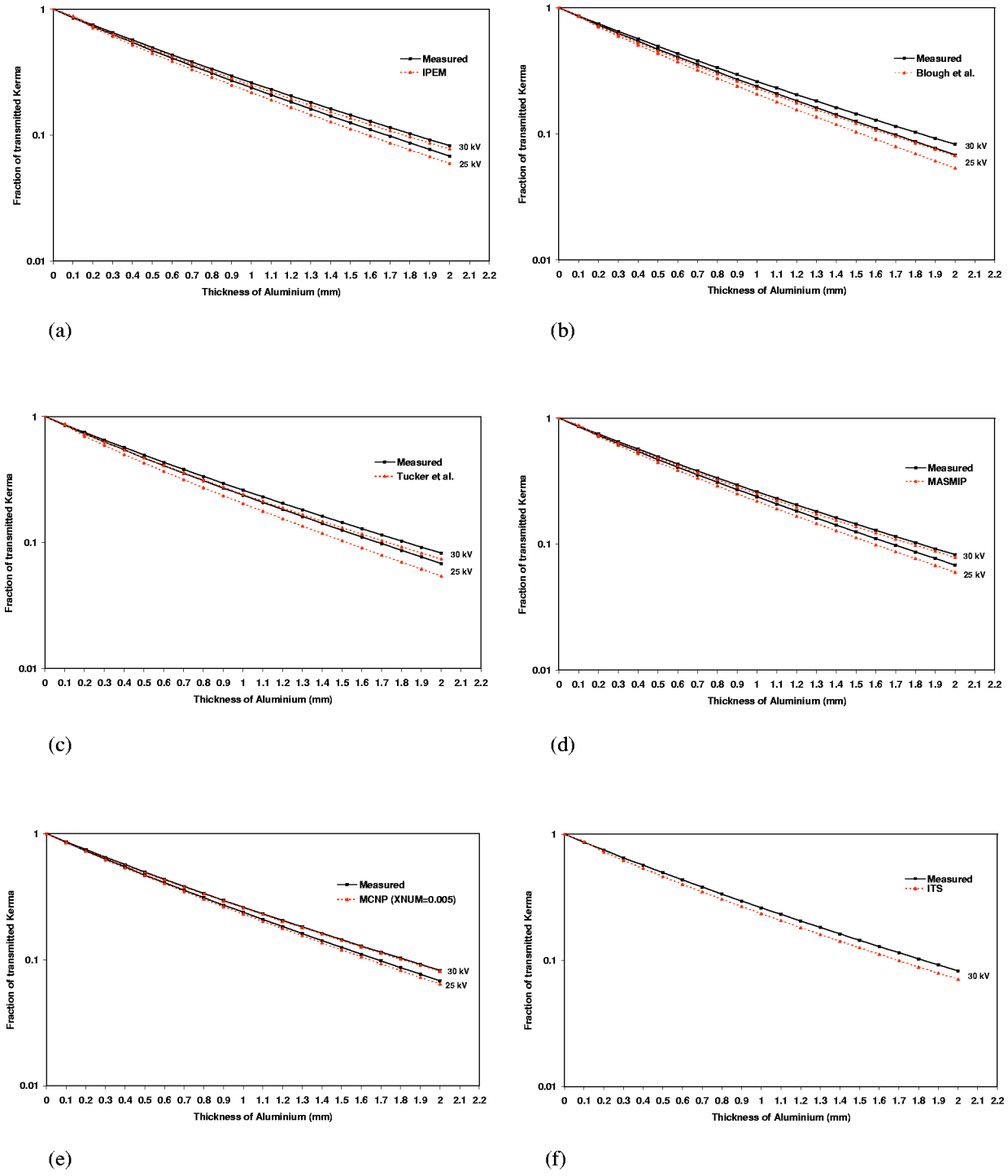

FIG. 4. Comparison of transmission curves produced by different computational models with those calculated from measured spectra at tube voltages 25 and 30 kV for 12° molybdenum target, 0.6 mm Al_{eq} inherent filter, 0.03 mm Mo additional filter, and FSD 100 cm.

ITS, and 12.6% at 35 kV, and 6.5% at 40 kV for XCOMP were observed. The MCNP4C transmission curve is in good agreement with the curve calculated from measured spectra. The mean and maximum differences are 3%, 5.7%, 1.1%, and 1.8% at tube voltages of 25 and 30 kV, respectively. This good agreement is obvious in calculation of HVLs where the difference with measured data is minimum for MCNP4C spectra, that is, 4.3% and 4% at tube voltages of 25 and 30 kV, respectively. The same observations can be made regarding the RMSD in the mammographic energy range where the MASMIP model for the molybdenum target results in the lowest values owing to the fact that it is based on unpublished spectral data that are similar but more recent than the reference spectra used in this work (Table IV).[9] IPEM performs well compared to other computational models for both molybdenum and tungsten targets.

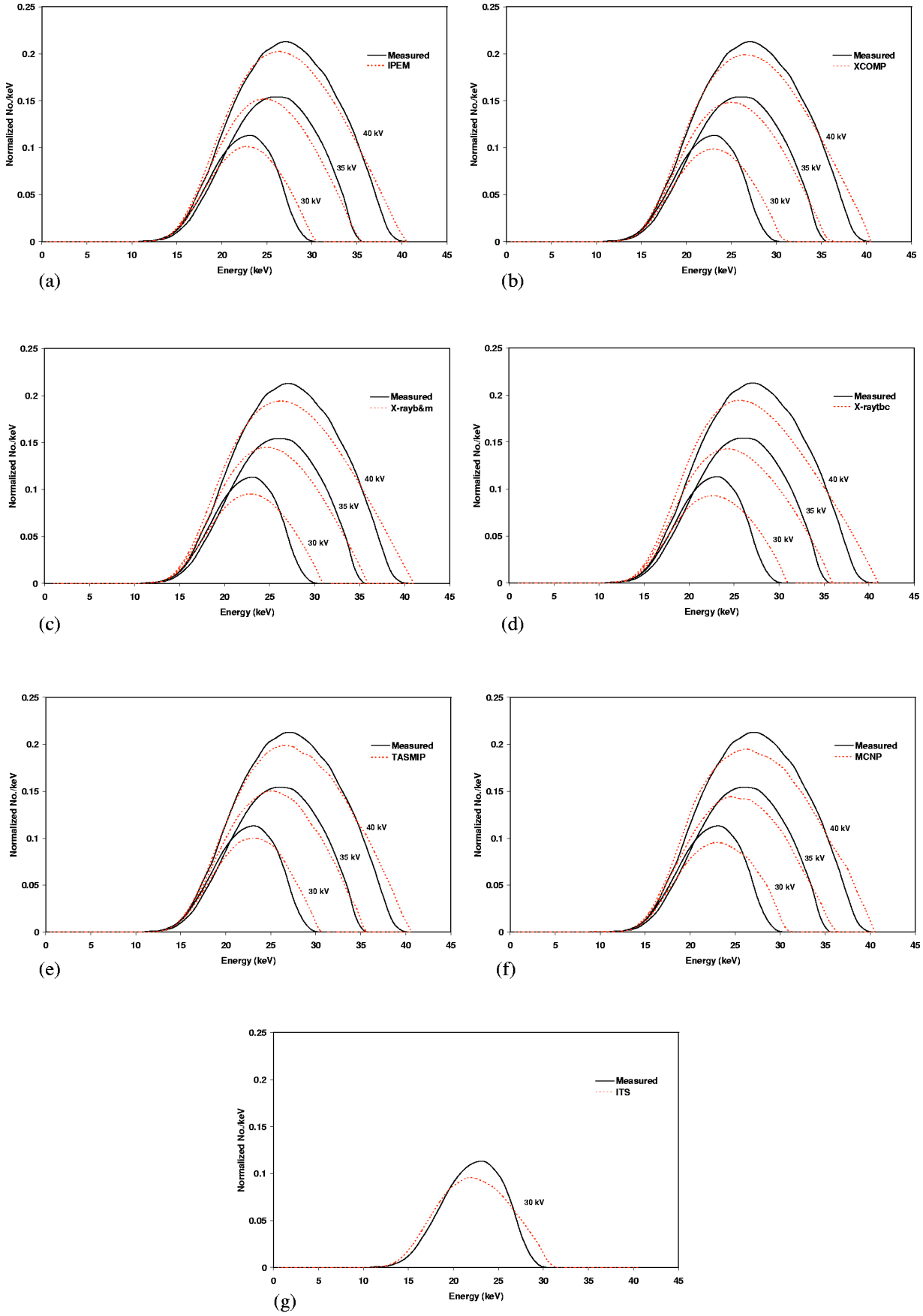

FIG. 5. Comparison of x-ray spectra calculated using different computational models with measured spectra at tube voltages 30, 35, and 40 kV for 12° tungsten target, 0.6 mm Al_{eq} inherent filter, 1.02 mm Al additional filter, and FSD 100 cm.

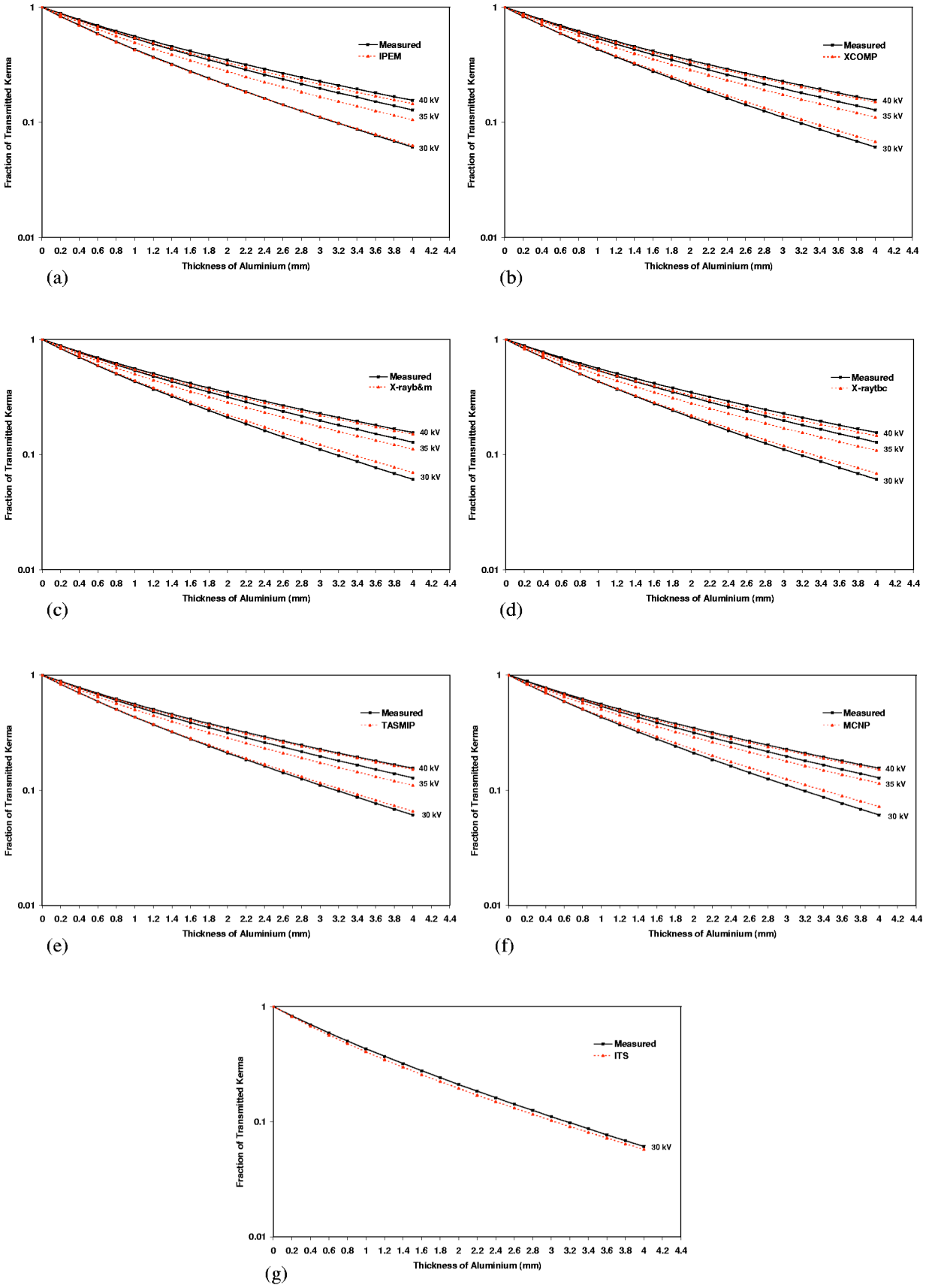

FIG. 6. Comparison of transmission curves produced by different computational models with those calculated from measured spectra at tube voltages 30, 35, and 40 kV for 12° tungsten target, 0.6 mm Al_{eq} inherent filter, 1.02 mm Al additional filter, and FSD 100 cm.

TABLE VII. Comparison between ratios of total molybdenum K x rays to sum of bremsstrahlung and K x rays obtained using measured and calculated spectra for different tube voltages. The MCNP4C calculations include results obtained using two values for the XNUM parameter of the PHYS:E card, which is used to control the sampling of x-ray photons produced along electron substeps (the default value XNUM=1 corresponds to the case where an analog number of tracks is sampled).

Computational model	25 kV		30 kV	
	Total	Difference (%)	Total	Difference (%)
Measured	0.2992	na	0.3983	na
IPEM	0.2860	1.1	0.4160	−4.4
Blough *et al.*	0.3470	−19.9	0.3200	19.6
Tucker *et al.*	0.2230	22.9	0.4000	−0.4
MASMIP	0.2310	20.1	0.3460	13.1
MCNP4C[a]	0.4970	−71.8	0.5230	−31.3
MCNP4C[b]	0.5020	−73.5	0.5670	−42.3
ITS3.0	⋯	⋯	0.3500	12.1

[a]XNUM=0.0005.
[b]XNUM=1.

The Monte Carlo calculations of mean breast absorbed dose ($\overline{D_b}$) and ED in typical mammography imaging setup using different computational models for generating x-ray spectra in the adult ORNL hermaphroditic phantom at 30 kV are summarized in Table X. The maximum difference in calculation of $\overline{D_b}$ and Ed in molybdenum target is 2.5% and 2.6% when using the Blough *et al.* model, while this value is 1.5% and 1.1% for the X-raytbc tungsten target model.

IV. DISCUSSION

The differences in the bremsstrahlung x-ray energy distribution calculated by different semi-empirical models in comparison with measured spectra can be explained by the differences in the fitting equations derived in these models for prediction of spectra. Different semi-empirical polynomial functions used in these models are the origin of the discrepancy in the production of bremsstrahlung x-ray intensity. The comparison of these functions shows that the Birch and Marshal models (IPEM, XCOMP, and X-rayb&m) produce less low energy photons and more high energy photons compared to the Tucker *et al.* model (X-raytbc). This behavior is obvious in Fig. 1. The different target geometry used in these models should be considered especially for low energy photons. In the Tucker *et al.* model, the electrons hit the target at angle 90° while this angle is $90-\theta$ (θ is the target angle) in the Birch and Marshal model. Thus, the photons produced in depth x pass through anode thickness $d=x/\tan\theta$ in the Birch and Marshal model and $d'=x/\sin\theta$ in the Tucker *et al.* model. The ratio d'/d shows that the Tucker model overestimates the target attenuation, which varies from 0.7% to 6% for a target angle between 7° and 20° (2.4% in our study with 12.5° target angle). Although the target absorption is an important parameter in the intensity of low energy photons, the difference in the semi-empirical polynomial functions compensate this effect in low-energy photon intensity. The spectra predicted by the TASMIP empirical model are in excellent agreement with measured spectra. The difference in K x-ray intensity is the result of arranging the data in 2 keV energy bins. It should, however, be emphasized that the same measured data were used for fitting interpolating polynomials. During the comparison of the calculated and measured spectra, especially the intensity of low photon energies, it is worth noticing that all models used a perfectly smooth target, while the influence of anode roughness on low energy photons in measured spectra appears to be important, especially at low tube voltages.[45]

The intensity of K x rays in the spectra is another important parameter that should be taken into account when comparing different computational models. Even though the semi-empirical models used an empirical relationship for the intensity of characteristic x rays,[30] they relied on different experimental measurements for adjusting their intensity. The difference in K x-ray yield in comparison with measured

TABLE VIII. Comparison of maximum and mean absolute relative difference between measured and calculation transmission curves in mammography energy range for molybdenum (12° target angle, 0.6 mm Al_{eq} inherent and 0.03 mm molybdenum additional filter) and tungsten targets (12° target angle, 0.6 mm Al_{eq} inherent and 1.02 mm Al additional filter).

Computational model	Mo target				W target					
	25 kV		30 kV		30 kV		35 kV		40 kV	
	Mean (%)	Max (%)	Mean (%)	Max (%)	Mean (%)	Max (%)	Mean (%)	Max (%)	Mean (%)	Max (%)
IPEM	7.6	12.1	4.0	5.8	1.0	3.3	11.1	17.6	4.2	6.4
Blough *et al.*	12.1	21.2	11.3	18.7	⋯	⋯	⋯	⋯	⋯	⋯
Tucker *et al.*	12.6	20.3	6.7	10.1	⋯	⋯	⋯	⋯	⋯	⋯
MASMIP	7.2	11.8	3.3	4.7	⋯	⋯	⋯	⋯	⋯	⋯
MCNP4C	3.0	5.7	1.1	1.8	8.0	18.7	7.2	10.1	2.6	6.2
ITS3.0	⋯	⋯	9.1	14.1	5.8	7.6	⋯	⋯	⋯	⋯
XCOMP			⋯	⋯	5.0	11.8	8.5	13.5	2.5	3.4
X-rayb&m					6.4	15.0	8.6	12.8	2.7	3.4
X-raybc					4.8	12.8	10.1	14.9	4.6	6.1
TASMIP					3.1	8.1	8.8	13.8	1.9	2.5

TABLE IX. Comparison between measured and computed HVL estimates (in mm Al) using the different computational models for tube voltages in mammography energy range for molybdenum (12° target angle, 0.6 mm Al_{eq} inherent and 0.03 mm molybdenum additional filter) and tungsten targets (12° target angle, 0.6 mm Al_{eq} inherent and 1.02 mm Al additional filter).

	Mo target				W target					
	25 kV		30 kV		30 kV		35 kV		40 kV	
Computational model	HVL	Difference (%)	HVL	Difference (%)	HVL	Difference (%)	HVL	Difference (%)	HVL	Difference (%)
Measured	0.46	na	0.50	na	0.81	na	1.11	na	1.22	na
IPEM	0.42	8.7	0.47	6.0	0.80	1.2	0.98	11.7	1.15	5.7
Blough *et al.*	0.41	10.9	0.47	6.0	⋯	⋯	⋯	⋯	⋯	⋯
Tucker *et al.*	0.40	13.0	0.46	8.0	⋯	⋯	⋯	⋯	⋯	⋯
MASMIP	0.42	8.7	0.47	6.0	⋯	⋯	⋯	⋯	⋯	⋯
MCNP4C	0.44	4.3	0.48	4.0	0.82	−1.2	1.07	3.6	1.17	4.1
ITS3.0	⋯	⋯	0.44	12.0	0.74	8.6	⋯	⋯	⋯	⋯
XCOMP			⋯	⋯	0.80	1.2	0.97	12.6	1.14	6.5
X-rayb&m					0.84	−3.7	1.01	9.0	1.17	4.1
X-raytbc					0.82	−1.2	0.99	10.8	1.14	6.5
TASMIP					0.81	0	1.00	9.9	1.18	3.2

spectra decreases with increasing tube voltage owing to the fact that all semi-empirical models were adjusted with measured spectra at 140 kV. Even though the same measured data were used for adjusting the characteristic x rays in X-raytbc and X-rayb&m, the lower intensity in X-raytbc is the effect of target absorption discussed above. Characteristic photons in MCNP are created by the electron impact ionization (EII) process. It has been shown that this model overestimates the total number of EII characteristic photons especially in mammography energy range.[19,21] The low characteristic x-ray intensity in the EGS4 spectra can be explained by the fact that the contribution of electron impact ionization had not been included in the EGS4 code system at the time of simulation.[4]

All semi-empirical models based on Birch and Marshal theory (IPEM, XCOMP, and X-rayb&m) produce spectra with higher quality than measured spectra, while the situation is reversed in the model based on the Tucker *et al.* theory (X-raytbc). This is due to production of softer x-ray spectra in the Tucker *et al.* model. We have considered the aluminum equivalent thickness needed to match TASMIP with the Fewell spectra,[10] so that the attenuation curve calculated from TASMIP spectra is in good agreement. The transmission curves calculated from MCNP4C spectra are higher than those obtained from measured spectra because of the overestimation of K x rays and high energy bremsstrahlung photons ($E > 68$ keV) in the spectra, while the EGS4 spectra produce a lower transmission curve compared to the measured one because of underestimation of K x rays.

The calculation of absorbed dose and ED in the ORNL hermaphroditic phantom from the spectra generated by different models was used to assess the effect of spectra in the

TABLE X. Comparison between MCNP4C-based Monte Carlo calculations of mean absorbed dose to the breasts ($\overline{D_b}$) and effective dose (ED) in adult ORNL hermahroditic phantom for typical mammography imaging setup of 30 kV in Mo target (FSD 50 cm, 12° target angle, 0.6 mm Al_{eq} inherent filter and 0.03 mm Mo additional filter) and W target (FSD 50 cm, 12° target angle, 0.6 mm Al_{eq} inherent and 1.02 mm Al additional filter). The standard deviatin (SD) in calculation of mean absorbed dose to the breasts is negligible.

	Mo target				W target			
Computational model	$\overline{D_b}$ (mGy)	Difference (%)	ED (μSv)	Difference (%)	$\overline{D_b}$ (mGy)	Difference (%)	ED (μSv)	Difference (%)
Measured	2.00	na	104.37±22.1	na	2.00	na	104.05±13.6	na
IPEM	1.99	0.5	103.70±7.6	0.6	2.00	0.0	104.05±15.7	0.0
Blough *et al.*	1.95	2.5	101.70±22.2	2.6	⋯	⋯	⋯	⋯
Tucker *et al.*	1.97	1.5	103.00±21.3	1.3	⋯	⋯	⋯	⋯
MASMIP	2.00	0.0	104.40±7.5	0.0	⋯	⋯	⋯	⋯
MCNP4C	2.00	0.0	104.40±22.1	0.0	2.01	−0.5	104.62±12.9	−0.5
ITS3.0	1.96	2.0	102.30±8.8	2.0	1.98	1.0	102.89±13.1	1.1
XCOMP	⋯	⋯	⋯	⋯	2.01	−0.5	104.62±12.9	−0.5
X-rayb&m					1.98	1.0	102.89±13.2	1.1
X-raytbc					1.97	1.5	102.89±13.1	1.1
TASMIP					2.01	−0.5	104.62±15.6	−0.5

field of radiation dosimetry. The calculated ED from the X-raytbc model results in lower estimates compared to spectra generated by other models. Similar results were reported by Caon *et al.*[35] The underestimation of ED observed with 3.2 mm aluminium filter is the effect of absorption of soft x rays in the filter. The magnitude of the relative difference increases more substantially with increasing filtration thickness for the spectra generated by the models based on Birch and Marshal theory since they produce less soft x rays than measured spectra.

The comparative assessment of x-ray spectra generated by different computational models to measured spectra for molybdenum target showed that the Blough *et al.* and Tucker *et al.* models produce more soft energy than IPEM for the reasons discussed previously. The discrepancy between the Blough *et al.* model and measured spectra at 25 kV probably is due to the overestimation of the Dyson derivation[46] or to slight differences in the implementation of this model at this energy.[6] The difference between MASMIP and measured spectra is attributed to the fact that different measured spectra were used for interpolating polynomials.[9] Comparison of the MCNP4C spectra with measured spectra showed that the code highly overestimates the production of K x rays with the default setting (XNUM=1). The optimal adjustment of the XNUM parameter in the PHYS:E card proved to be a difficult issue. Further investigation showed that MCNP produces bremsstrahlung energy distribution in good agreement with measured spectra. The discrepancy shown in Fig. 3 results from spectral normalization with overestimated characteristic x-ray peaks.[19] The simulated spectra with ITS3.0 showed that this code gives a better approximation of K x rays in comparison with MCNP4C, although the electron physics enhancement library was intended to make MCNP4C more consistent with ITS 3.0. It is worth emphasizing that the K-shell impact ionization calculation (based upon ITS 3.0) remains unchanged with el03 evaluation.[39] The latter uses detailed calculations of the electron-nucleus bremsstrahlung cross section for electrons with energies below 2 MeV and above 50 MeV. According to Fig. 5, the spectrum peak in all semi-empirical models occurred in lower energy and with less intensity than the measured spectra. One plausible explanation could be the overestimation of electron penetration in the target in the Thomson-Whiddington relation[30] where the range of electrons is proportional to T_0^2 below 50 keV while it is proportional to T_0 for higher energies (T_0 is the kinetic energy of electron). The systematic discrepancy between measured and calculated transmission curves is the result of systematic differences between the corresponding spectra in both molybdenum and tungsten target spectra in the mammography energy range.

Despite there not being any statistically significant differences between measured and calculated spectra for all computational models considered in this study, the flexibility and robustness of these models with respect to generating the desired spectrum for a variety of parameters such as target material, target angle, additional fitter, tube voltage ripple, and energy bin and accurate modeling of more recent x-ray generator designs should be considered. The empirical models are inherently limited in terms of target angle and filter material as well as tube voltage ripple in the mammography energy range. Although semi-empirical models are more flexible compared to empirical models, they are limited to specific target materials, particular sets, or combinations of additional filters and voltage ripples. Notwithstanding, there is no theoretic limitation in the prediction of x-ray spectra for the different parameters mentioned above using the Monte Carlo method; computer proficiency and computational time remain the challenges for widespread application of Monte Carlo simulations. With the advent of high speed parallel supercomputers, which have much higher execution rates, and recent developments in Grid technology allowing us to subdivide time-consuming simulations on geographically distributed platforms, the field has received increased attention and will certainly live up to its potential in the near future.

V. CONCLUSION

The spectra generated using a number of different computational models were compared with measured spectra. The comparative assessment showed that the energy distribution and the quality of spectra produced by the Tucker model (X-raytbc) are in better agreement with measured spectra than other models in the diagnostic radiology energy range while IPEM has better agreement in the mammography energy range. The empirical models perform well since they are based on the reference experimental spectra used in this work. It should, however, be emphasized that these models are rather limited in terms of flexibility with respect to target angle and filter material. MCNP4C has good agreement with experimental measurements in the diagnostic radiology energy range, while ITS3.0 reproduces more accurately the measured spectra in the mammography energy range. Although Monte Carlo modeling is time consuming, the simulations provide detailed information about the interactions inside the target and filter, which can be useful for the design of new target/filter combinations, for instance in transmission x-ray tube design.[47]

ACKNOWLEDGMENTS

This work was supported by the Department of Physics & Nuclear Sciences (AmirKabir University of Technology) and the Swiss National Science Foundation under Grant No. SNSF 3152A0-102143. The authors would like to thank Dr. J. M. Boone, Dr. M. Bhat, Dr. K. P. Ng, Dr. L. E. Wilkinson, Dr. G. Stirling, Dr. R. Nowotny, and Dr. G. W. Allen who shared with us their data and programs.

[a)]Electronic mail: farshid.ay@tppgems.com

[1]T. R. Fewell and R. E. Shuping, "Handbook of mammographic x-ray spectra," HEW publication (FDA) 79–8071, 1978.
[2]T. R. Fewell, R. E. Shuping, and K. E. Healy, "Handbook of computed tomography x-ray spectra," HHS publication (FDA), 81–8162, 1981.
[3]M. Bhat, J. Pattison, G. Bibbo, and M. Caon, "Diagnostic x-ray spectra: a comparison of spectra generated by different computational methods with a measured spectrum," Med. Phys. **25**, 114–120 (1998).
[4]M. Bhat, J. Pattison, G. Bibbo, and M. Caon, "Off-axis x-ray spectra: a

comparison of Monte Carlo simulated and computed x-ray spectra with measured spectra," Med. Phys. **26**, 303–309 (1999).
[5]D. R. Dance *et al.*, "Influence of anode/filter material and tube potential on contrast, signal-to-noise ratio and average absorbed dose in mammography: a Monte Carlo study," Br. J. Radiol. **73**, 1056–1067 (2000).
[6]L. E. Wilkinson, P. N. Johnston, and J. C. Heggie, "A comparison of mammography spectral measurements with spectra produced using several different mathematical models," Phys. Med. Biol. **46**, 1575–1589 (2001).
[7]T. R. Fewell and R. E. Shuping, "Photon energy distribution of some typical diagnostic x-ray beams," Med. Phys. **4**, 187–197 (1977).
[8]B. R. Archer and L. K. Wagner, "Determination of diagnostic x-ray spectra with characteristic radiation using attenuation analysis," Med. Phys. **15**, 637–641 (1988).
[9]J. M. Boone, T. R. Fewell, and R. J. Jennings, "Molybdenum, rhodium, and tungsten anode spectral models using interpolating polynomials with application to mammography," Med. Phys. **24**, 1863–1874 (1997).
[10]J. M. Boone and J. A. Seibert, "An accurate method for computer-generating tungsten anode x-ray spectra from 30 to 140 kV," Med. Phys. **24**, 1661–1670 (1997).
[11]R. G. Waggnere *et al.*, "X-ray spectra estimation using attenuation measurements from 25 kVp to 18 MV," Med. Phys. **26**, 1269–1278 (1999).
[12]R. Birch and M. Marshall, "Computation of bremsstrahlung X-ray spectra and comparison with spectra measured with a Ge(Li) detector," Phys. Med. Biol. **24**, 505–517 (1979).
[13]R. Nowotny and A. Hofer, "Ein program fur die berechnung von diagnostic Rontgenspektren," Fortschr Rontgenstr. **142**, 685–689 (1985).
[14]W. J. Iles, "The Computation of the bremsstrahlung x-ray spectra over an energy range 15 keV to 300 keV," Report NRPB-R204 National Radiological Protection Board, 1987.
[15]D. M. Tucker, G. T. Barnes, and D. P. Chakraborty, "Semiempirical model for generating tungsten target x-ray spectra," Med. Phys. **18**, 211–218 (1991).
[16]D. M. Tucker, G. T. Barnes, and X. Z. Wu, "Molybdenum target x-ray spectra: A semiempirical model," Med. Phys. **18**, 402–407 (1991).
[17]M. M. Blough, R. G. Waggener, W. H. Payne, and J. A. Terry, "Calculated mammographic spectra confirmed with attenuation curves for molybdenum, rhodium, and tungsten targets," Med. Phys. **25**, 1605–1612 (1998).
[18]R. N. Kulkarni and S. J. Supe, "Monte Carlo calculations of mammographic x-ray spectra," Phys. Med. Biol. **29**, 185–190 (1984).
[19]M. R. Ay, M. Shahriari, S. Sarkar, M. Adib, and H. Zaidi, "Monte Carlo simulation of x-ray spectra in diagnostic radiology and mammography using MCNP4C," Phys. Med. Biol. **49**, 4897–4917 (2004).
[20]K. P. Ng, C. S. Kwok, and F. H. Tang, "Monte Carlo simulation of x-ray spectra in mammography," Phys. Med. Biol. **45**, 1309–1318 (2000).
[21]F. Verhaegen, A. E. Nahum, S. Van de Putte, and Y. Namito, "Monte Carlo modeling of radiotherapy kV x-ray units," Phys. Med. Biol. **44**, 1767–1789 (1999).
[22]L. Silberstein, "Determination of the spectral composition of x-ray radiation from filtration data," Opt. Soc. Am. **22**, 265–280 (1932).
[23]B. W. Soole, "A determination of x-ray attenuation analysis for approximating the intensity distribution at its point of origin of bremsstrahlung excited in a thick target by incidenct electrons of constant medium energy," Phys. Med. Biol. **21**, 369–389 (1976).
[24]B. R. Archer, T. R. Fewell, and L. K. Wager, "Laplace reconstruction of experimental diagnostic x-ray spectra," Med. Phys. **15**, 832–837 (1988).
[25]P. Huang, T. Chen, and K. R. Kase, "Reconstruction of diagnostic x-ray spectra by numerical analysis of transmission data," Med. Phys. **13**, 707–710 (1986).
[26]P. Francois, A. Catala, and Ch. Scouarnec, "Simulation of x-ray spectra reconstruction from transmission data by direct resolution of the numeric system AF=T," Med. Phys. **20**, 1695–1703 (1993).
[27]J. M. Boone, "X-ray spectral reconstruction from attenuation data using neural networks," Med. Phys. **17**, 647–654 (1990).
[28]J. M. Boone, "The three parameter equivalent spectra as an index of beam quality," Med. Phys. **15**, 304–310 (1988).
[29]H. A. Kramers, "On the theory of x-ray absorption and of the continuous x-ray spectrum," Philos. Mag. **46**, 836–871 (1923).
[30]M. Green and V. E. Cosslett, "Measurements of K, L and M shell x-ray production efficiencies," Br. J. Appl. Phys. **1**, 425 (1968).
[31]A. Vignes and G. Dez, "Distribution in depth of the primary x-ray emission in anticathodes of titanium and lead," Br. J. Appl. Phys. **1**, 1309–1322 (1968).
[32]J. R. Mercier *et al.*, "Modification and benchmarking of MCNP for low-energy tungsten spectra," Med. Phys. **27**, 2680–2687 (2000).
[33]M. R. Ay, S. Sarkar, M. Shahriari, D. Sardari, and H. Zaidi, "Comparative assessment of different computational models for generation of x-ray spectra in diagnostic radiology and mammography," Proc. IEEE Nuclear Science Symposium and Medical Imaging Conference, 19–22 October, Rome, Italy (2004) (in press).
[34]J. P. Bissonnette and L. J. Schreiner, "A comparison of semiempirical models for generating tungsten target x-ray spectra," Med. Phys. **19**, 579–582 (1992).
[35]M. Caon, G. Bibbo, J. Pattison, and M. Bhat, "The effect on dose to computed tomography phantoms of varying the theoretical x-ray spectrum: a comparison of four diagnostic x-ray spectrum calculating codes," Med. Phys. **25**, 1021–1027 (1998).
[36]R. Birch, M. Marshall, and G. M. Ardran, Catalogue of Spectral Data for Diagnostic X-Rays Hospital Physicists, Report SRS30, 1979.
[37]M. J. Berger and J. H. Hubbell, XCOM: Photon cross sections on a personal computer, National Bureau of Standards (US), Report NBSIR 87-3597, 1987.
[38]K. Cranley, B. J. Gilmore, G. W. A. Fogarty, and L. Desponds, IPEM Report 78 Catalogue of Diagnostic X-Ray Spectra and other Data, The Institute of Physics and Engineering in Medicine (IPEM); CD-Rom Edition 1997 (Electronic Version prepared by D. Sutton), 1997.
[39]J. F. Briesmeister, "MCNP—A general Monte Carlo N-particle transport code," version 4C, Los Alamos National Laboratory, NM, Report LA-13709-M, 2000.
[40]W. R. Nelson, H. Hirayama, and D. Roger, The EGS4 code system, Stanford Linear Accelerator Center, Report SLAC-256, 1985.
[41]J. A. Halbleib *et al.*, "ITS Version 3.0: The Integrated TIGER," series of coupled Electron/Photon Monte Carlo Transport Codes, Sandia National Laboratories, Report SAND91-1634, 1992.
[42]M. Cristy and K. F. Eckerman, "Specific Absorbed Fractions of Energy at Various Ages from Internal Photon Source," Report ORNL/TM-8381/V1-7, Oak Ridge National Laboratory, 1987.
[43]ICRP Report 60, Recommendations of the International Commission on Radiological Protection, International Commission on Radiological Protection, 1991.
[44]NRPB, A National Survey of Doses to Patients Undergoing a Selection of Routine X-ray Examination in English Hospitals. Report R200, National Radiological Protection Board, 1986.
[45]R. Nowotny and Kh. Meghzifene, "Simulation of the effect of anode surface roughness on diagnostic x-ray spectra," Phys. Med. Biol. **47**, 3973–3983 (2002).
[46]N. A. Dyson, *X-ray in Atomic and Nuclear Physics*, 2nd ed. (Cambridge University Press, Cambridge, 1990).
[47]L. M. N. Tavora, E. J. Morton, and W. B. Gilboy, "Design considerations for transmission x-ray tubes operated at diagnostic energies," J. Phys. D **33**, 2497–2507 (2000).